Angewandte Chemie
Eine Zeitschrift der Gesellschaft Deutscher Chemiker

Supporting Information

How Photoisomerization Drives Peptide Folding and Unfolding: Insights from QM/MM and MM Dynamics Simulations

Shu-Hua Xia, Ganglong Cui, Wei-Hai Fang, and Walter Thiel**

anie_201509622_sm_miscellaneous_information.pdf

Contents

List of Figures

List of Tables

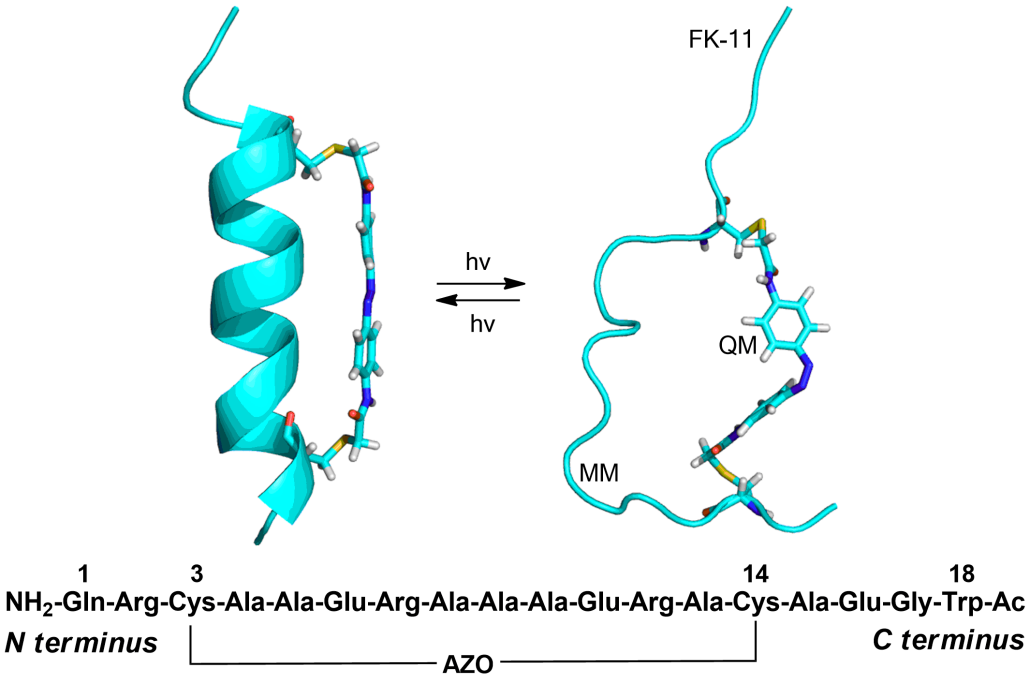

Figure 1: The FK-11 peptide in the α-helix (left) and random-coil (right) conformations. In the QM/MM computations, the QM region consists of the azobenzene cross-linker, while the MM region is comprised of all the other atoms (residues and water). Also shown is the sequence of the FK-11 peptide.

1 Computational Methods

1.1 Diabatic Surface-Hopping Method

In this work we adopt the diabatic surface-hopping method to simulate the initial cis-trans and trans-cis photoisomerization processes of the azobenzene cross-linked FK-11 peptide (Fig. 1). Robb and coworkers [1–3] proposed this method to model nonadiabatic transitions near conical intersections. In this approach, two conditions must be satisfied for a hop to occur from an upper to a lower state: (1) the energy difference between these two states must be less than a predefined threshold (T_1=10 kcal/mol presently); (2) the system must pass a conical intersection. The energy difference can be easily calculated using available electronic structure packages that support excited-state calculations; however, judging whether the system is passing a conical intersection is more involved. Here we adopt a simple scheme that is specified in the following using an S_1-S_0 surface hop as an example. $C_i(1)$ and $C_i(0)$ refer to the state vectors of S_1 and S_0 at MD step i; whereas $C_{i-1}(1)$ and $C_{i-1}(0)$ represent the state vectors of S_1 and S_0 at MD step i-1. If the system is passing a conical intersection from step i-1 to i, both $C_i(1)$*$C_{i-1}(1)$ and $C_i(0)$*$C_{i-1}(0)$ should be smaller than a predefined threshold (T_2 < 0.5 presently); and both $C_i(0)$*$C_{i-1}(1)$ and $C_i(1)$*$C_{i-1}(0)$ should be larger (T_3 > 0.5 presently).

1.2 System Setup

Initial structures of the azobenzene cross-linker in the cis and trans forms and of the FK-11 peptide in the α-helix and random-coil conformations were constructed using the PYMOL package. [4] The azobenzene cross-linker was then manually attached to the two cysteine residues of the peptide in the α-helix and random-

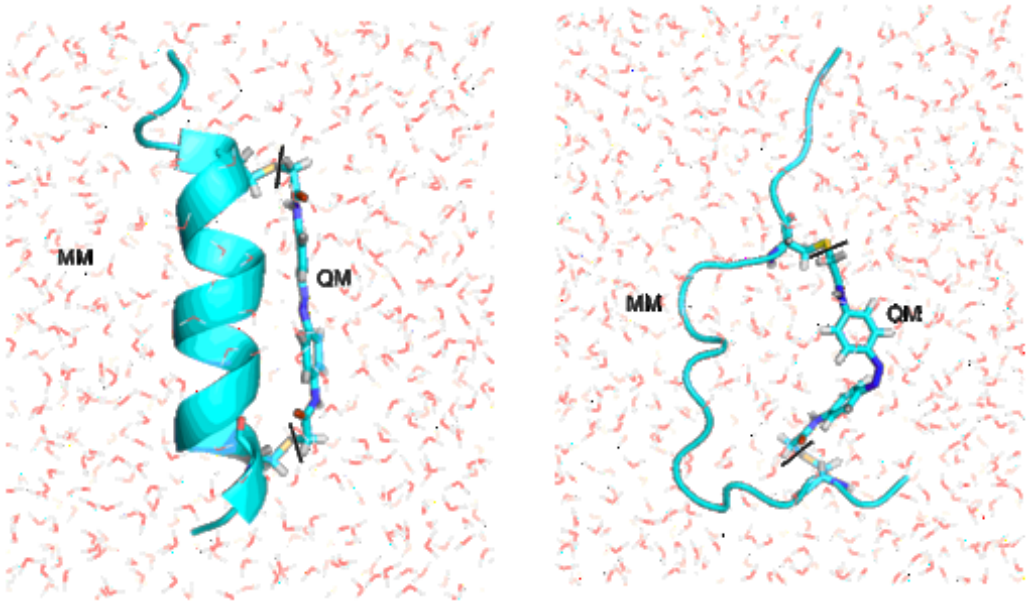

Figure 2: Solvated (left) trans-helix and (right) cis-coil systems. See text for the details of system setup.

coil conformations. Finally, the two systems were solvated in cubic water boxes of 60 and 53 Å diameter, respectively (Fig. 2).

1.3 QM/MM Method

All QM/MM computations [5, 6] were carried out using GROMACS4.5 [7] interfaced to GAUSSIAN03. [8] The QM subsystem comprised the azobenzene cross-linker (38 atoms), while the MM subsystem was composed of all peptide residues and water molecules (22269 and 14982 atoms for the α-helix and random-coil peptide, respectively). The QM subsystem was described using the complete active space self-consistent field (CASSCF) method. As a compromise between computational efficiency and accuracy, we adopted in all CASSCF computations an active space of six electrons distributed over four orbitals and an economic 3-21G* basis set. [9, 10] These choices for the active space and the basis set had been validated and applied in previous ab initio nonadiabatic dynamics simulations of azobenzene in solution. [11–13] The MM subsystem was represented using the AMBER03 force field (peptide residues) [14] and the SPC water model. [15] The QM-MM boundary was treated by the hydrogen link-atom scheme. [16] The QM-MM electrostatic interactions were handled by the electronic embedding scheme. [17] The QM-MM van der Waals interactions were computed as pairwise Lennard-Jones interactions, [18] with a cutoff of 10 Å. Periodic boundary conditions were applied; the MM-MM electrostatic interactions were evaluated using the fourth-order particle-mesh Ewald (PME) algorithm [19] and a grid spacing of 1.0 Å. Fig. 1 illustrates the QM/MM partition in our QM/MM calculations.

1.4 Benchmark of the CASSCF Method

Full-dimensional ab initio nonadiabatic dynamics simulations are very expensive, in particular at the QM/MM level when including tens of thousands of MM atoms; thus, we must adopt a compromise between compu-

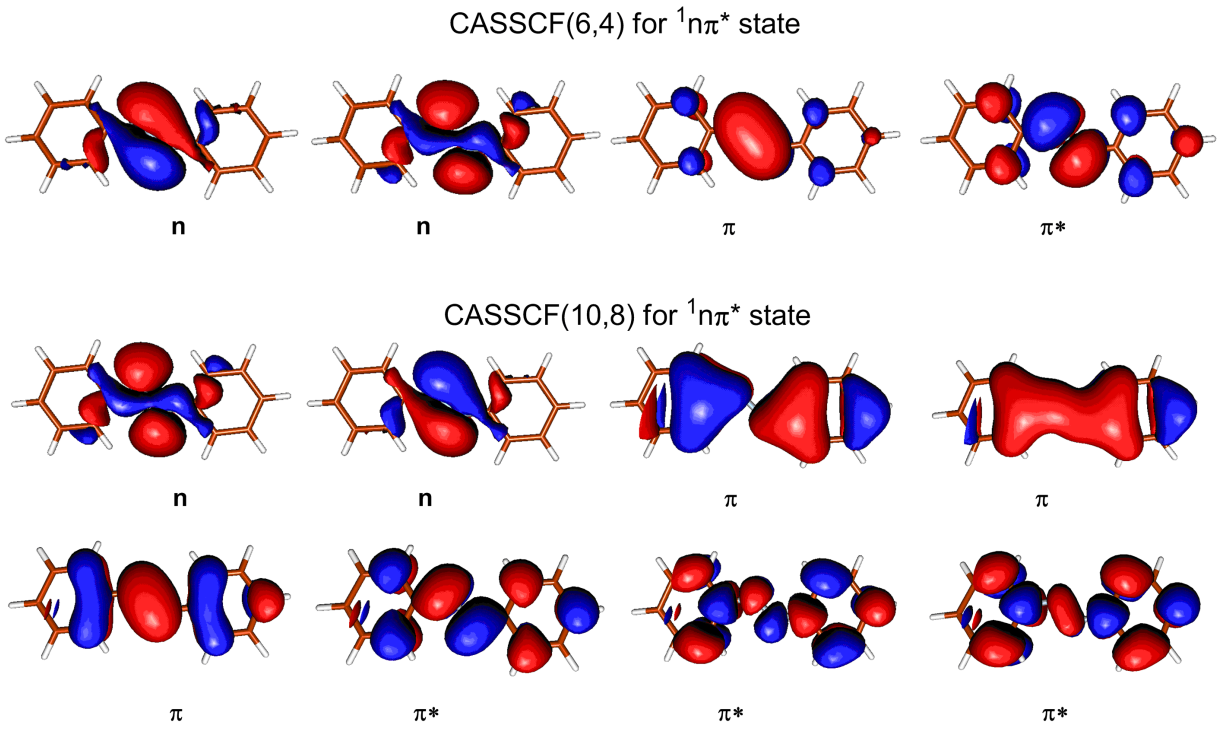

Figure 3: Active spaces used in the (top) CASSCF(10,8) and (bottom) CASSCF(6,4) calculations, respectively. Each active space includes both lone-pair orbitals from the two N atoms.

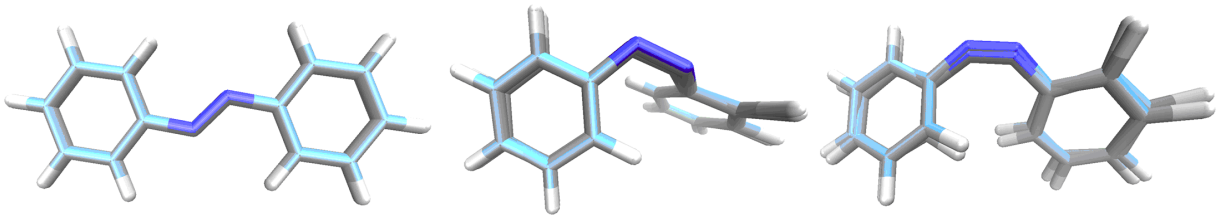

Figure 4: Overlay of the CASSCF(6,4)/3-21G* and CASSCF(10,8)/6-31G* optimized S_1 structures with the CNNC dihedral angle constrained to 180°, 90°, and 0°, respectively.

tational efficiency and accuracy. In the present work, we use CASSCF calculations with an active space of six electrons distributed over four orbitals and an economic 3-21G* basis set. [9, 10] This computational protocol has been validated and applied in previous ab initio nonadiabatic dynamics simulations of azobenzene in solution, which demonstrated that it is reasonably accurate. [12, 13] Specifically, it was shown for azobenzene that this level of theory provides accurate structures for the S_0 and S_1 minima and the S_1/S_0 conical intersections, which are close to those obtained by the CASSCF(10,8)/6-31G* method (see Supporting Information in ref. [13]) as well as reasonably accurate energies compared with those computed at the CASPT2//CASSCF(10,8)/6-31G* level (see the second paragraph of the "Results and Discussion" section of ref. [13]).

The topology of the ground-state and excited-state potential energy surfaces plays a key role in full-dimensional dynamics simulations. To further validate the chosen CASSCF approach, we have computed the S_1 minimum-energy photoisomerization paths by constrained optimization at the CASSCF(6,4)/3-21G*

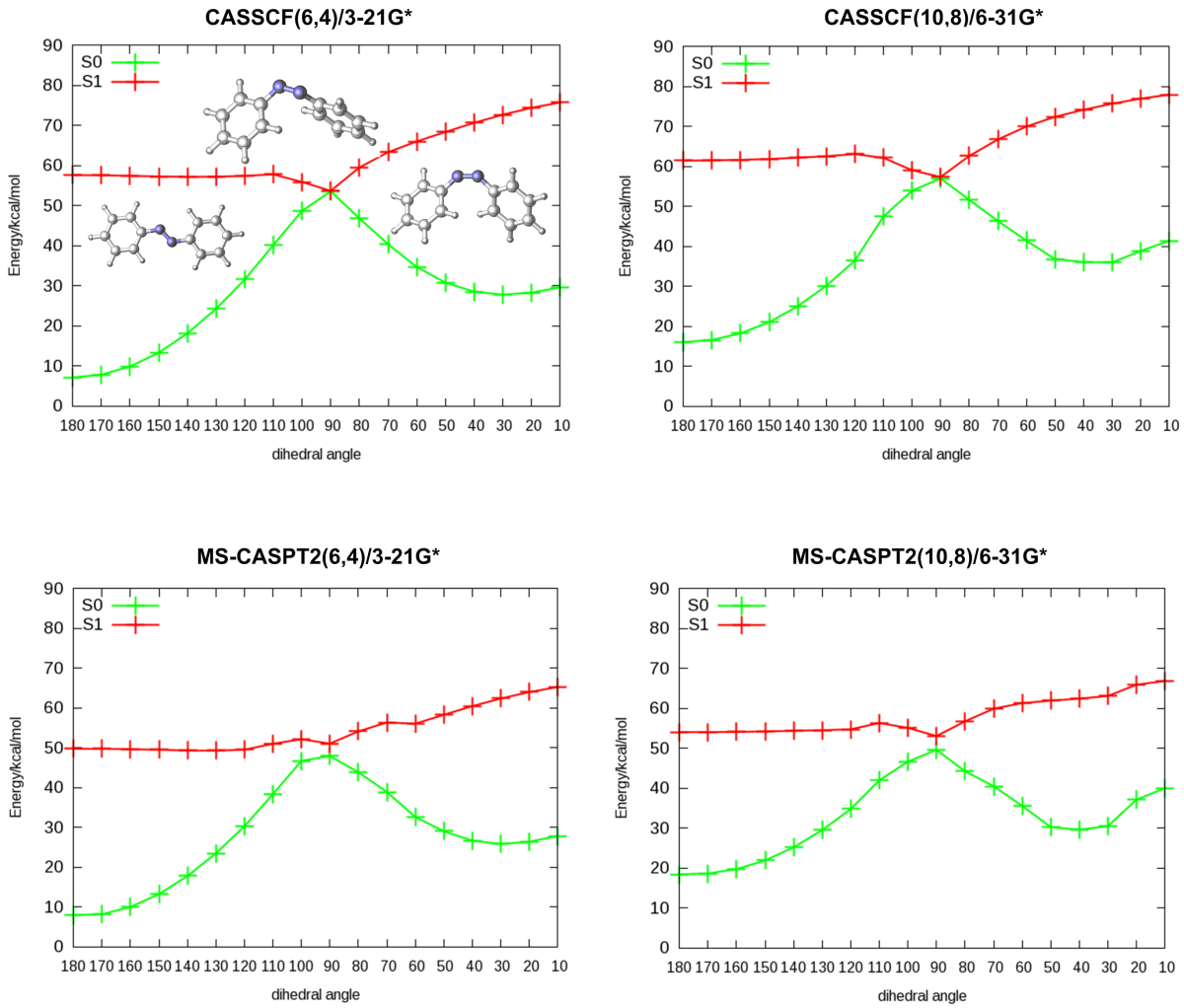

Figure 5: Energy profiles along the photoisomerization paths of azobenzene (relaxed S_1 in red and unrelaxed S_0 in green) obtained from optimizations using (top-left) CASSCF(6,4)/3-21G* and (top-right) CASSCF(10,8)/6-31G* and from corresponding single-point calculations using (bottom-left) MS-CASPT2(6,4)/3-21G* and (bottom-right) MS-CASPT2(10,8)/6-31G*. In each case, the S_0 minimum energy at 180^0 is chosen as reference point.

and CASSCF(10,8)/6-31G* levels. Furthermore, we have refined the predicted energies through single-point MS-CASPT2(6,4)/3-21G* and MS-CASPT2(10,8)/6-31G* calculations, respectively. Fig. 3 shows the chosen active spaces for the CASSCF(6,4)/3-21G* and CASSCF(10,8)/6-31G* computations. In both cases, they include the two lone-pair orbitals at the two nitrogen atoms because our target S_1 state is of nπ character, as shown in many previous theoretical studies. [20–28] All other orbitals are of π or π^* character.

Fig. 5 collects the S_1 energy profiles along the photoisomerization paths of azobenzene computed at the CASSCF(6,4)/3-21G*, CASSCF(10,8)/6-31G*, MS-CASPT2(6,4)/3-21G*, and MS-CASPT2(10,8)/6-31G* methods, along with the corresponding unrelaxed S_0 energy profiles. It is evident that the topology of the two CASSCF-based profiles is essentially the same (top panel) indicating that the extension of the active space and basis set has very little effect on the relative energies; specifically, the S_1 energies from CASSCF(6,4)/3-21G* are consistently slightly lower than those from CASSCF(10,8)/6-31G* (by 2-3 kcal/mol). The overall shape of the energy profiles from the single-point MS-CASPT2 calculations (bottom panel) is qualitatively similar to that of their CASSCF-based counterparts, with a general downward shift by about 8 kcal/mol (which does not affect the overall topology). We have also checked the CASSCF(6,4)/3-21G* and CASSCF(10,8)/6-31G* optimized S_1 geometries along the S_1 photoisomerization paths: both approaches give essentially the same structures, as demonstrated in Fig. 4 for three examples (CNNC dihedral angle constrained to 180°, 90°, and 0°).

In summary, the quoted previous and the present benchmarks show that the economic CASSCF(6,4)/3-21G* approach gives a reasonably accurate description of the photoisomerization of azobenzene, which validates its use in nonadiabatic dynamics simulations.

1.5 QM/MM Dynamics

Each prepared system was first energy-minimized and then subjected to a 3 ps ground-state equilibrium dynamics simulation. Initial conditions for the subsequent QM/MM diabatic surface-hopping dynamics simulations were randomly sampled from this trajectory. In the present study, we performed 20 and 14 runs to model the cis-trans and trans-cis photoisomerization processes of the azobenzene cross-linked FK-11 peptide. The required energies, gradients, and state vectors were computed “on the fly” at the QM/MM level. Nuclear coordinates were integrated using the velocity Verlet algorithm with a time step of 2 fs. [29] All MM bond lengths involving hydrogen atoms were constrained using the LINCS algorithm. [30] The QM/MM diabatic surface-hopping trajectories were terminated 200 fs after the system had hopped to the S_0 state.

1.6 MM Molecular Dynamics

Classical MD simulations were employed to explore the photoinduced folding and unfolding dynamics of the azobenzene cross-linked FK-11 peptide. In order to analyze the effects of the initial photoisomerization on the dynamics, initial conditions for these classical MD simulations (i.e. atomic coordinates and velocities) were randomly sampled from the QM/MM trajectories that had successfully completed the cis-trans or trans-cis photoisomerization and had decayed to the S_0 state. Specifically, 70 and 46 trajectories were extracted

for the cis-trans induced folding dynamics and the trans-cis induced unfolding dynamics, respectively. The AMBER03 force field [14] and the SPC model [15] were employed to describe the peptide residues and the water molecules. The azobenzene cross-linker was modeled based on the force field proposed by Böckmann and coworkers. [31]

In the classical MD simulations, all bond lengths involving hydrogen atoms were constrained using the LINCS algorithm; [30] the temperature was kept at 300 K using the Berendsen thermostat; [32] and the velocity Verlet algorithm was used to integrate the nuclear equations of motion with a 2 fs time step. [29] All MD simulations and analyses were carried out using the GROMACS4.5 package. [7]

2 Hopping Times and Energy Gaps at Hopping Points

Table 1 collects $S_1 \rightarrow S_0$ hopping times and S_1-S_0 energy gaps at all hopping points, and specifies the final azobenzene conformation in all nonadiabatic dynamics trajectories. We find that 11 of 20 (55%) cis-coil trajectories evolve into the trans-isomer of azobenzene, while 6 of 14 (43%) trans-helix trajectories evolve into the cis-isomer. On the basis of these results, we estimate the cis-trans and trans-cis quantum yields to be 0.55 and 0.43; given the small number of trajectories, these values are admittedly only crude estimates with large statistical uncertainties.

The average $S_1 \rightarrow S_0$ hopping time (69 fs) in the trajectories starting from the cis-coil conformation is much shorter than that in the trajectories starting from the trans-helix conformation (621 fs). This trend is consistent with available experimental and theoretical studies in vacuo or in solution, [26, 27, 33, 34] but the difference between the average hopping times is larger in the present case.

The S_1/S_0 energy gaps at the hopping points are mostly in the range between 1 and 5 kcal/mol (average value: 3.0 kcal/mol) indicating that the internal conversion occurs close to the conical intersection seam.

Table 1: Hopping time (fs), S_1/S_0 energy gap at the hopping point (kcal/mol), and final conformation of azobenzene linker as obtained from QM/MM nonadiabatic dynamics trajectories; runs 1-20 (21-34) start from the cis-isomer (trans-isomer) of azobenzene.

run	time	gap	result	run	time	gap	result
1	38	4.8	trans	18	120	2.1	trans
2	58	2.1	trans	19	138	4.2	trans
3	170	1.5	trans	20	71	3.4	trans
4	75	5.9	cis	21	1117	2.8	trans
5	82	2.6	trans	22	296	3.1	trans
6	53	2.6	cis	23	1196	1.3	trans
7	65	2.6	cis	24	849	1.8	trans
8	71	3.2	cis	25	929	1.1	cis
9	43	2.4	trans	26	411	3.7	cis
10	63	2.4	trans	27	683	2.8	trans
11	40	4.3	trans	28	420	1.0	trans
12	39	1.9	cis	29	494	3.2	cis
13	25	5.8	trans	30	450	2.1	cis
14	70	2.2	cis	31	356	1.9	trans
15	42	2.3	cis	32	382	3.2	cis
16	108	8.6	cis	33	332	2.7	trans
17	72	2.7	cis	34	775	1.7	cis

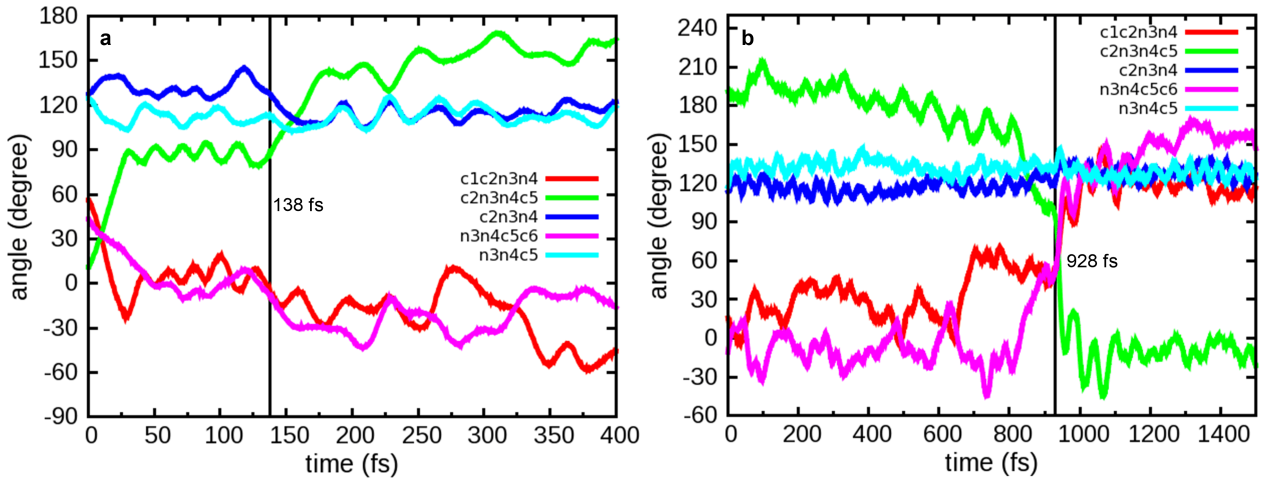

Figure 6: Time-dependent geometric parameters in two typical trajectories illustrating nonadiabatic cis-trans (a) and trans-cis (b) photoisomerizations. Further trajectories are shown in Section 4.

3 Two Typical Trajectories

In this section, we discuss two typical photoisomerization trajectories in some detail. The other trajectories are shown in Section 4 without further explanation.

Panel a of Fig. 6 shows the time-dependent evolution of five key geometric parameters in a typical trajectory for cis-trans photoisomerization. It starts from a cis-coil conformation with an initial central C2N3N4C5 dihedral angle of about 11°. Upon photoirradiation, this dihedral angle immediately increases to about 90° within around 25 fs, in conjunction with an almost synchronous decrease of the dihedral angles characterizing the phenyl torsions: C1C2N3N4 from 56° to -17° and C2N3N4C5 from 43° to 23°. By contrast, the C2N3N4 and N3N4C5 bending angles merely fluctuate slightly. In this run, the system does not decay to the S_0 state when it first approaches the S_1/S_0 conical intersection region after 25 fs; instead it oscillates for more than 100 fs (ca. 2.5 vibrational periods) and then hops to the ground state at 138 fs. Thereafter, the vibrationally "hot" system evolves toward the trans-coil conformation until the end of the QM/MM nonadiabatic dynamics simulations. Panel b shows data from a typical trajectory for trans-cis isomerization. One major difference from panel a is the much longer timescale: in the first 800 fs, the central C2N3N4C5 dihedral angle fluctuates around its initial value of 180°. During this period, the C1C2N3N4 and N3N4C5C6 dihedral angles describing the phenyl torsions oscillate strongly, by up to more than 60°. The S_1-S_0 trans-cis surface hop occurs at 928 fs and is accompanied by strong changes in all three dihedral angles (see Fig. 6).

4 Additional Figures

In this section, we first present snapshots from classical MD simulations of the FK-11 peptide without and with the azobenzene cross-linker taken from two trajectories without cross-linker (Fig. 7), from four folding trajectories with cross-linker (Fig. 8), and from five unfolding trajectories with cross-linker (Fig. 9). Thereafter we show the time evolution of key angles in all 34 available nonadiabatic dynamics trajectories (Figs. 7-11).

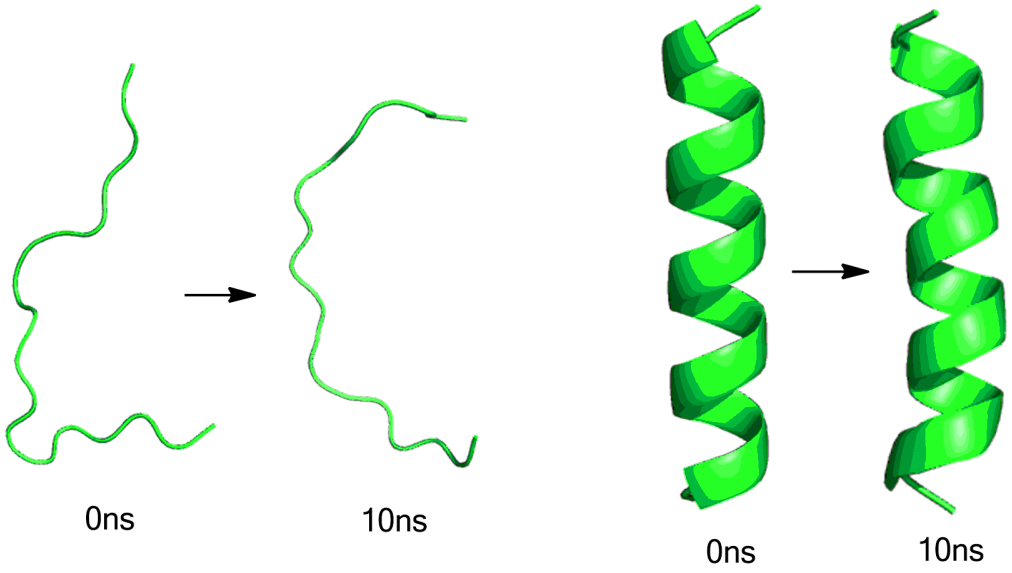

Figure 7: Two snapshots of a typical trajectory of the FK-11 peptide without the azobenzene cross-linker.

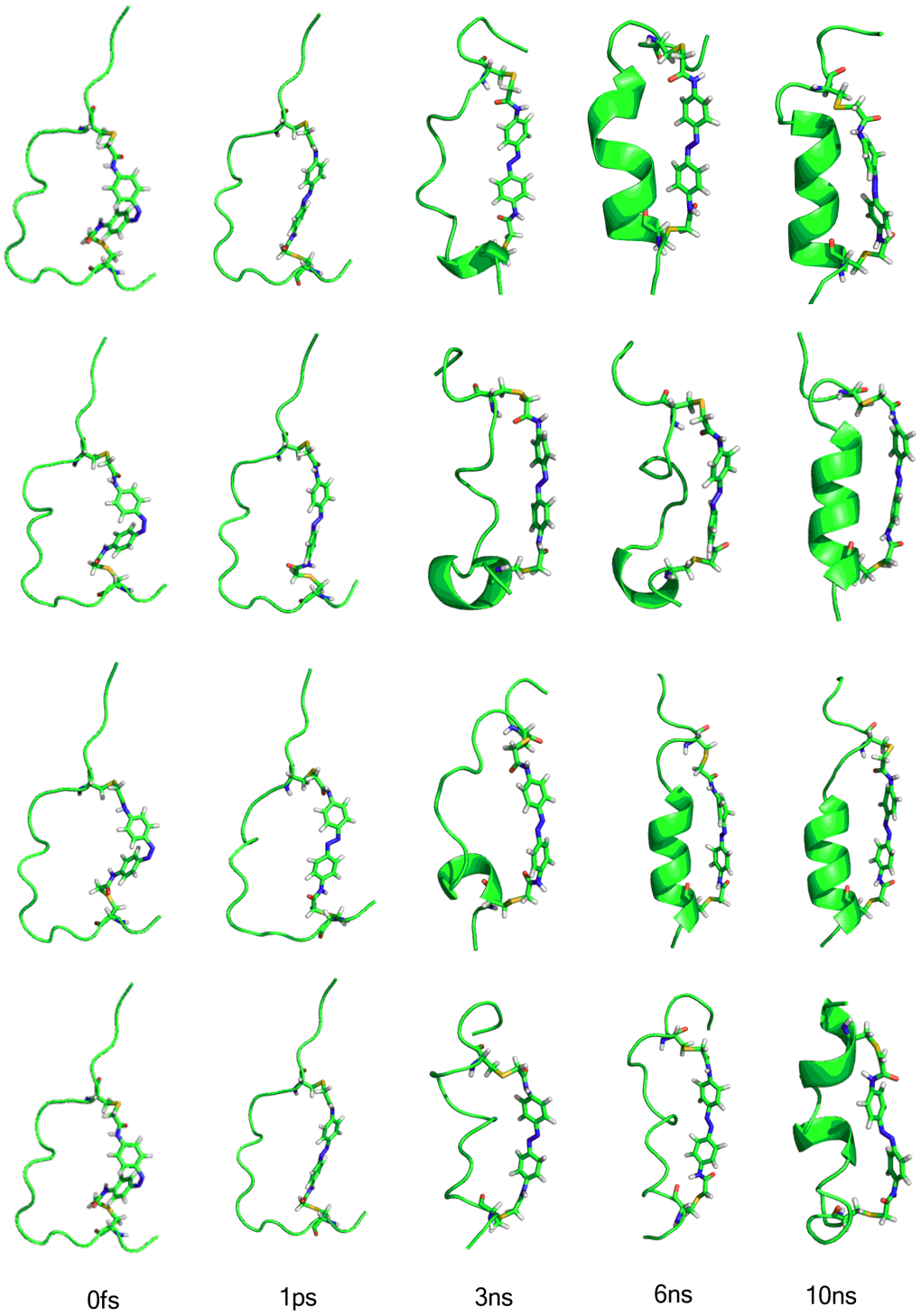

Figure 8: Four folding trajectories of the FK-11 peptide with the azobenzene cross-linker simulated with our combined QM/MM and MM approach.

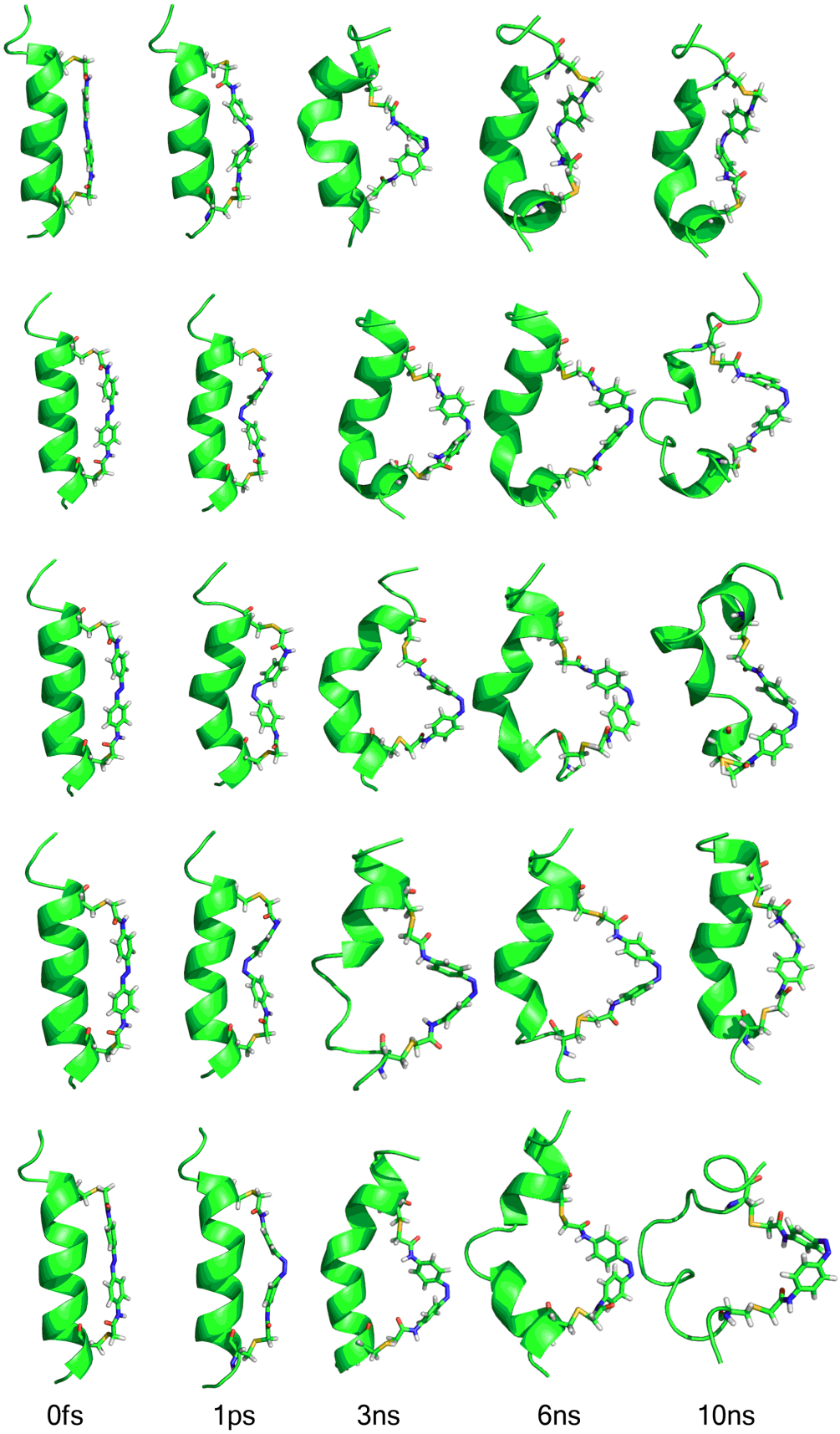

Figure 9: Five unfolding trajectories of the FK-11 peptide with the azobenzene cross-linker simulated with our combined QM/MM and MM approach.

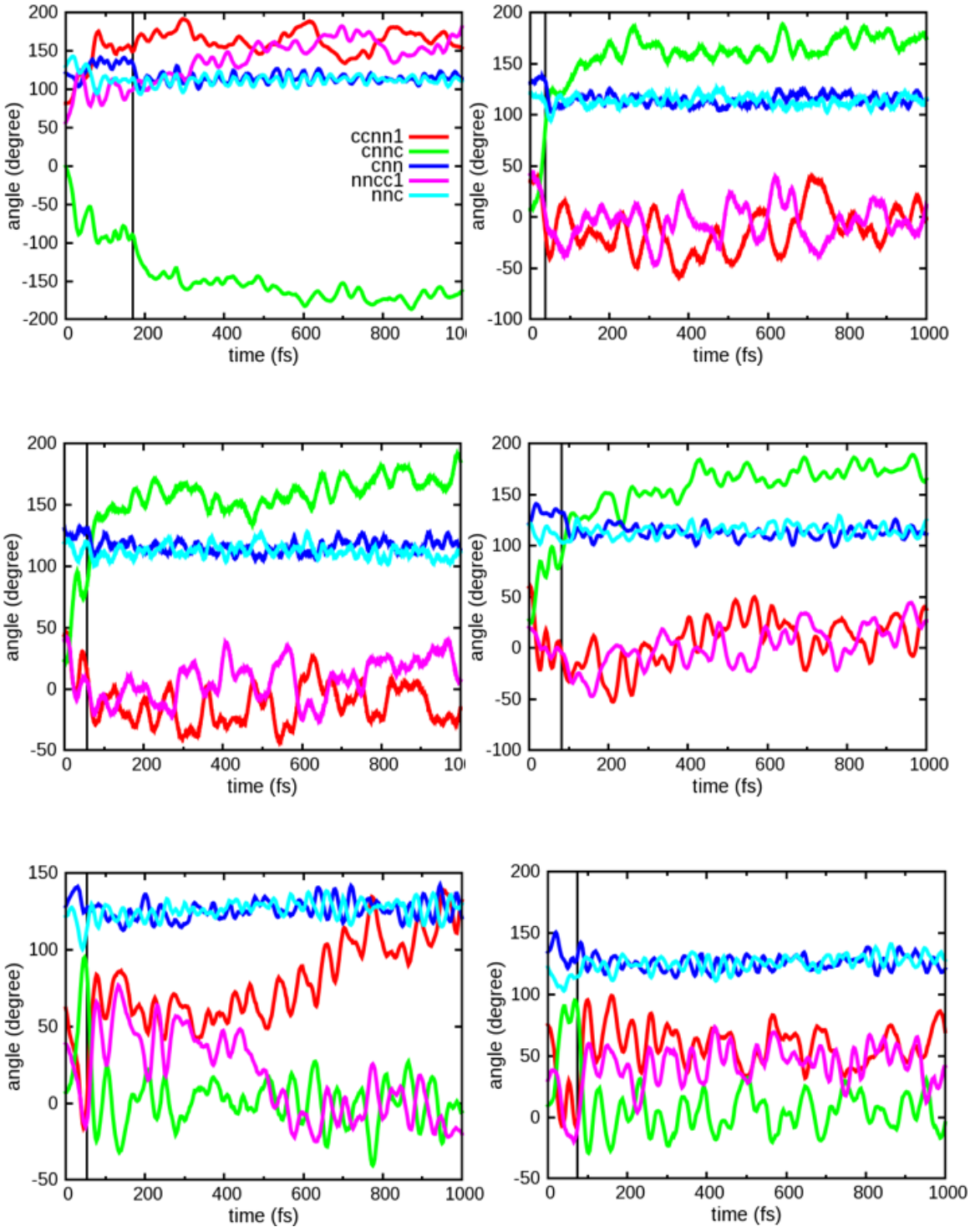

Figure 10: QM/MM nonadiabatic dynamics trajectories starting from the cis azobenzene: trajectories 1-6.

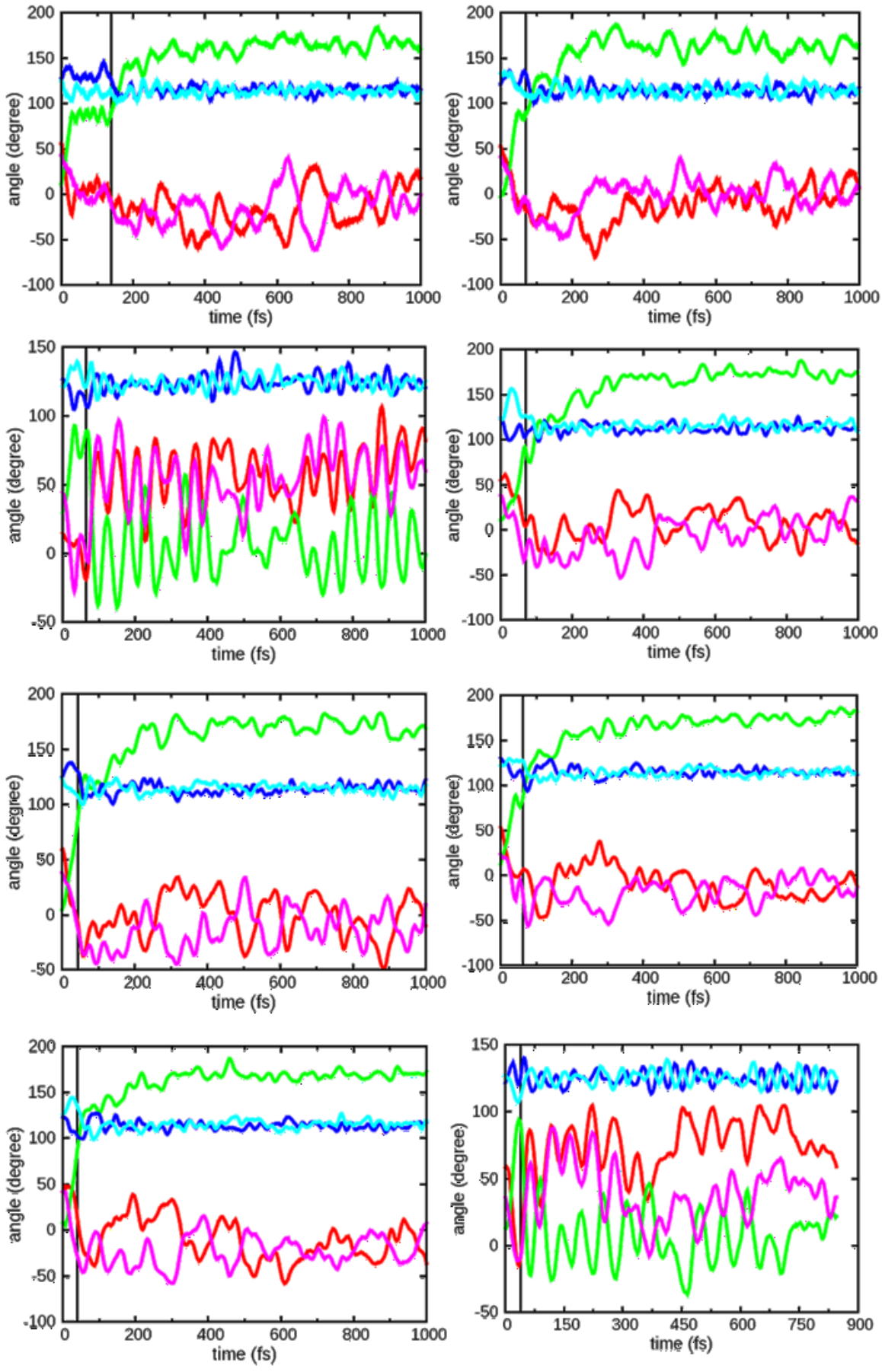

Figure 11: QM/MM nonadiabatic dynamics trajectories starting from the cis azobenzene: trajectories 7-14.

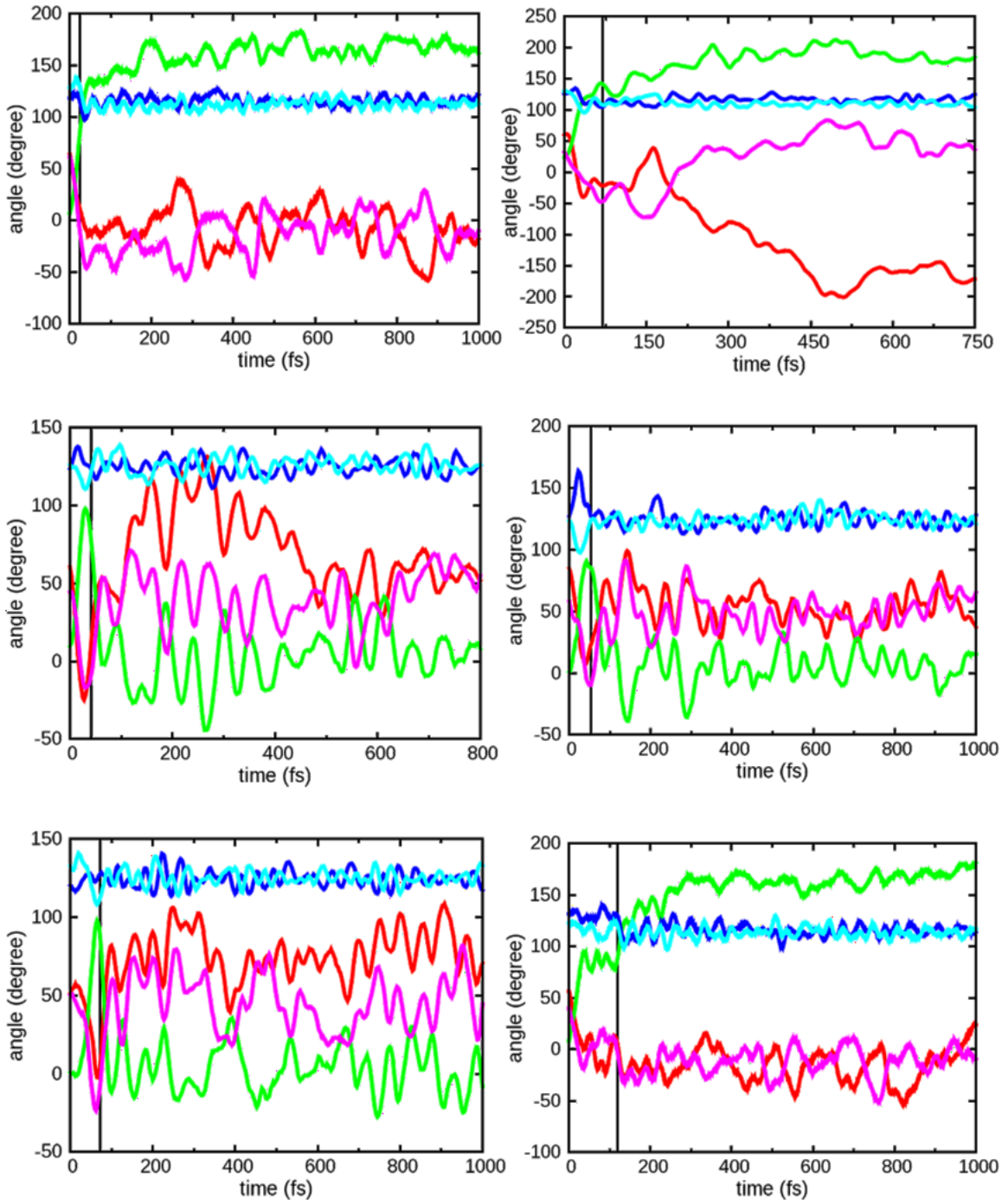

Figure 12: QM/MM nonadiabatic dynamics trajectories starting from the cis azobenzene: trajectories 15-20.

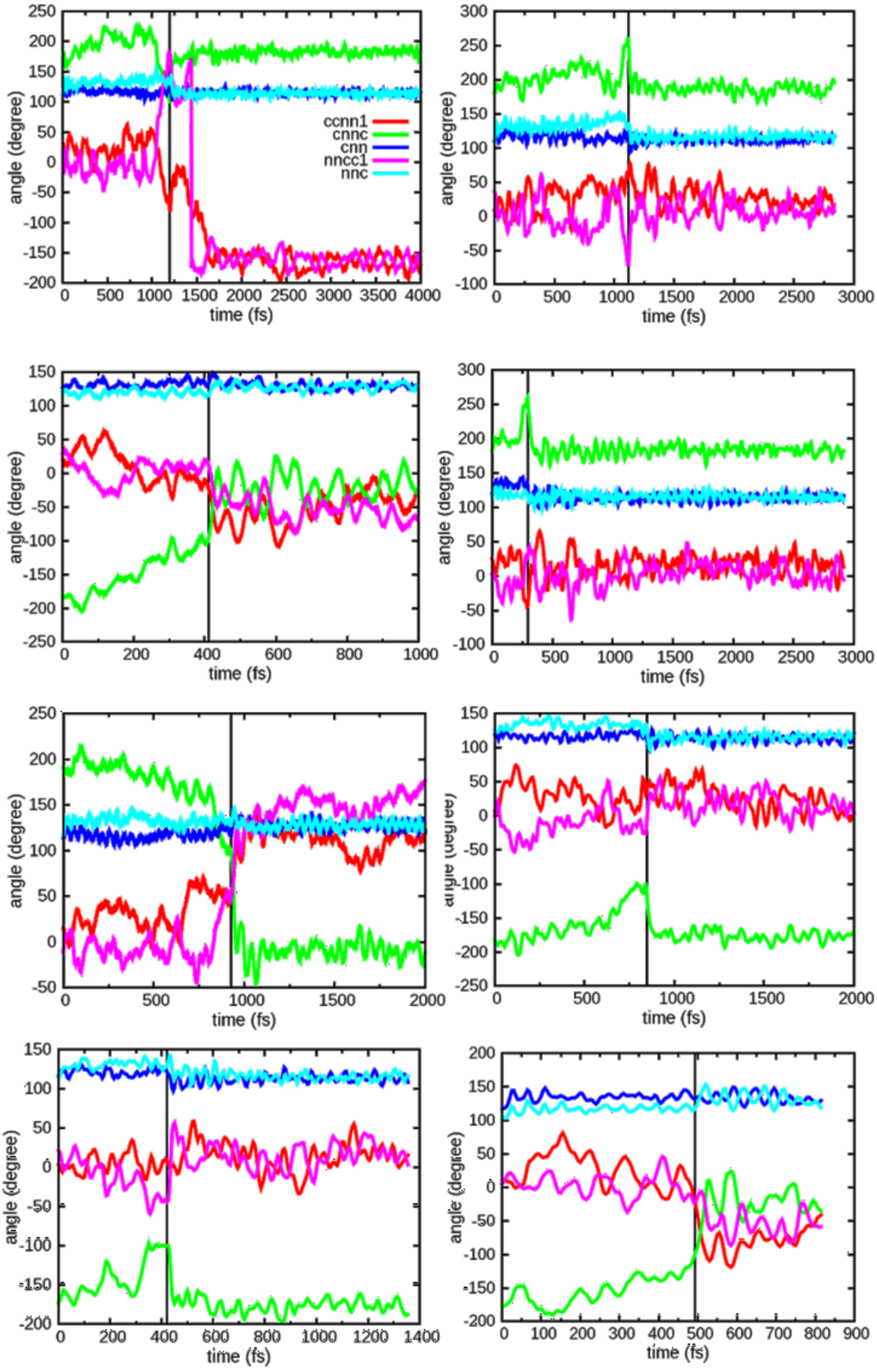

Figure 13: QM/MM nonadiabatic dynamics trajectories starting from the trans azobenzene: trajectories 1-8.

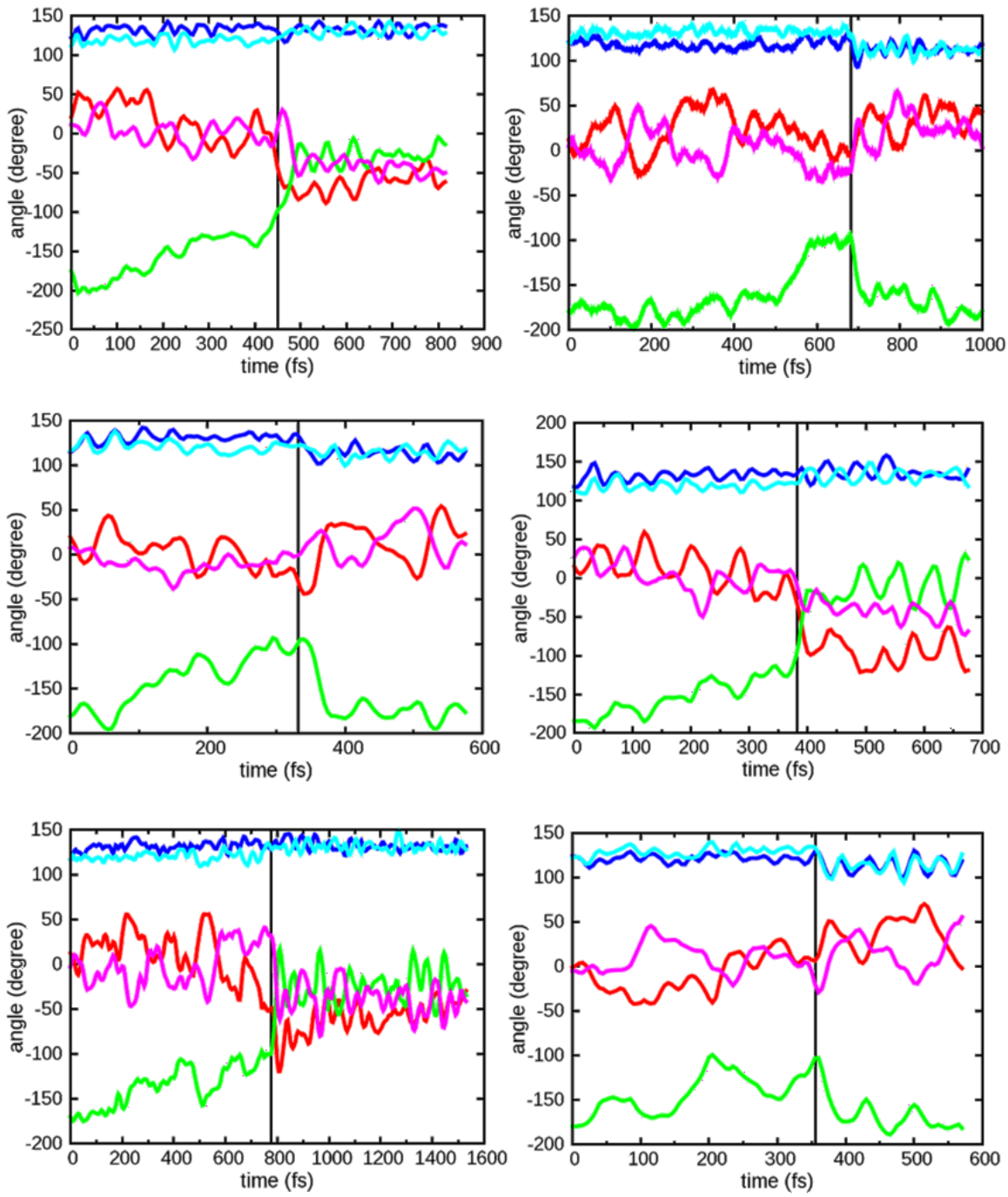

Figure 14: QM/MM nonadiabatic dynamics trajectories starting from the trans azobenzene: trajectories 9-14.

References

[1] G. Groenhof, M. Bouxin-Cademartory, B. Hess, S.P. De Visser, H.J.C. Berendsen, M. Olivucci, A.E. Mark, and M.A. Robb. Photoactivation of the photoactive yellow protein: why photon absorption triggers a trans-to-cis isomerization of the chromophore in the protein. *J. Am. Chem. Soc.*, 126(13):4228–4233, 2004.

[2] G. Groenhof, L.V. Schäfer, M. Boggio-Pasqua, H. Grubmüller, and M.A. Robb. Arginine52 controls the photoisomerization process in photoactive yellow protein. *J. Am. Chem. Soc.*, 130(11):3250–3251, 2008.

[3] M. Boggio-Pasqua, M.A. Robb, and G. Groenhof. Hydrogen bonding controls excited-state decay of the photoactive yellow protein chromophore. *J. Am. Chem. Soc.*, 131(38):13580–13581, 2009.

[4] W. L. DeLano. The PyMOL Molecular Graphics System. DeLano Scientific, San Carlos, CA, USA, 2002.

[5] A. Warshel and M. Karplus. Calculation of ground and excited state potential surfaces of conjugated molecules. I. Formulation and parametrization. *J. Am. Chem. Soc.*, 94(16):5612–5625, 1972.

[6] A. Warshel and M. Levitt. Theoretical studies of enzymic reactions: Dielectric, electrostatic and steric stabilization of the carbonium ion in the reaction of lysozyme. *J. Mol. Biol.*, 103:227–249, 1976.

[7] B. Hess, C. Kutzner, D. van der Spoel, and E. Lindahl. GROMACS 4: Algorithms for Highly Efficient, Load-Balanced, and Scalable Molecular Simulation. *J. Chem. Theory Comput.*, 4:435–447, 2008.

[8] M. J. Frisch, G. W. Trucks, H. B. Schlegel, G. E. Scuseria, M. A. Robb, J. R. Cheeseman, J. A. Montgomery, Jr., T. Vreven, K. N. Kudin, J. C. Burant, J. M. Millam, S. S. Iyengar, J. Tomasi, V. Barone, B. Mennucci, M. Cossi, G. Scalmani, N. Rega, G. A. Petersson, H. Nakatsuji, M. Hada, M. Ehara, K. Toyota, R. Fukuda, J. Hasegawa, M. Ishida, T. Nakajima, Y. Honda, O. Kitao, H. Nakai, M. Klene, X. Li, J. E. Knox, H. P. Hratchian, J. B. Cross, V. Bakken, C. Adamo, J. Jaramillo, R. Gomperts, R. E. Stratmann, O. Yazyev, A. J. Austin, R. Cammi, C. Pomelli, J. W. Ochterski, P. Y. Ayala, K. Morokuma, G. A. Voth, P. Salvador, J. J. Dannenberg, V. G. Zakrzewski, S. Dapprich, A. D. Daniels, M. C. Strain, O. Farkas, D. K. Malick, A. D. Rabuck, K. Raghavachari, J. B. Foresman, J. V. Ortiz, Q. Cui, A. G. Baboul, S. Clifford, J. Cioslowski, B. B. Stefanov, G. Liu, A. Liashenko, P. Piskorz, I. Komaromi, R. L. Martin, D. J. Fox, T. Keith, M. A. Al-Laham, C. Y. Peng, A. Nanayakkara, M. Challacombe, P. M. W. Gill, B. Johnson, W. Chen, M. W. Wong, C. Gonzalez, and J. A. Pople. Gaussian 03, Revision D.02. Gaussian, Inc., Wallingford, CT, 2004.

[9] J.S. Binkley, J.A. Pople, and W.J. Hehre. Self-consistent molecular orbital methods. 21. Small split-valence basis sets for first-row elements. *J. Am. Chem. Soc.*, 102(3):939–947, 1980.

[10] M.S. Gordon, J.S. Binkley, J.A. Pople, W.J. Pietro, and W.J. Hehre. Self-consistent molecular-orbital methods. 22. Small split-valence basis sets for second-row elements. *J. Am. Chem. Soc.*, 104(10):2797–2803, 1982.

[11] B.G. Levine and T.J. Martínez. Isomerization through conical intersections. *Annu. Rev. Phys. Chem.*, 58:613–634, 2007.

[12] L.-H. Liu, S. Yuan, W.-H. Fang, and Y. Zhang. Probing highly efficient photoisomerization of a bridged azobenzene by a combination of CASPT2//CASSCF calculation with semiclassical dynamics simulation. *J. Phys. Chem. A*, 115:10027–10034, 2011.

[13] J. Cao, L.H. Liu, W.H. Fang, Z.Z. Xie, and Y. Zhang. Photo-induced isomerization of ethylene-bridged azobenzene explored by ab initio based non-adiabatic dynamics simulation: A comparative investigation of the isomerization in the gas and solution phases. *J. Chem. Phys.*, 138:134306, 2013.

[14] Y. Duan, C. Wu, S. Chowdhury, M.C. Lee, G.M. Xiong, W. Zhang, R. Yang, P. Cieplak, R. Luo, and T.S. Lee. A point-charge force field for molecular mechanics simulations of proteins based on condensed-phase quantum mechanical calculations. *J. Comput. Chem.*, 24(16):1999–2012, 2003.

[15] H. J. C. Berendsen, J. P. M. Postma, W. F. Van Gunsteren, and J. Hermans. Interaction models for water in relation to protein hydration. In *Intermolecular forces*, pages 331–342. 1981.

[16] U.C. Singh and P.A. Kollman. A combined ab initio quantum mechanical and molecular mechanical method for carrying out simulations on complex molecular systems: applications to the CH3Cl+ Cl- exchange reaction and gas phase protonation of polyethers. *J. Comput. Chem.*, 7(6):718–730, 1986.

[17] H. M. Senn and W. Thiel. QM/MM Methods for Biomolecular Systems. *Angew. Chem. Int. Ed.*, 48:1198–1229, 2009.

[18] J.E. Jones. On the determination of molecular fields. ii. from the equation of state of a gas. *Proc. R. Soc. Lond. A*, 106:463–477, 1924.

[19] T. Darden, D. York, and L. Pedersen. Particle mesh Ewald: An Nlog (N) method for Ewald sums in large systems. *J. Chem. Phys.*, 98(12):10089–10092, 1993.

[20] T. Schultz, J. Quenneville, B. Levine, A. Toniolo, T.J. Martínez, S. Lochbrunner, M. Schmitt, J.P. Shaffer, M.Z. Zgierski, and A. Stolow. Mechanism and dynamics of azobenzene photoisomerization. *J. Am. Chem. Soc.*, 125:8098–8099, 2003.

[21] A. Cembran, F. Bernardi, M. Garavelli, L. Gagliardi, and G. Orlandi. On the mechanism of the cis-trans isomerization in the lowest electronic states of azobenzene: S_0, S_1, and T_1. *J. Am. Chem. Soc.*, 126:3234–3243, 2004.

[22] C. Ciminelli, G. Granucci, and M. Persico. The photoisomerization mechanism of azobenzene: A semiclassical simulation of nonadiabatic dynamics. *Chem. Eur. J.*, 10:2327–2341, 2004.

[23] L. Gagliardi, G. Orlandi, F. Bernardi, A. Cembran, and M. Garavelli. A theoretical study of the lowest electronic states of azobenzene: the role of torsion coordinate in the cis–trans photoisomerization. *Theor. Chem. Acc.*, 111:363–372, 2004.

[24] I. Conti, M. Garavelli, and G. Orlandi. The different photoisomerization efficiency of azobenzene in the lowest nπ^* and $\pi\pi^*$ singlets: the role of a phantom state. *J. Am. Chem. Soc.*, 130:5216–5230, 2008.

[25] T. Cusati, G. Granucci, and M. Persico. Photodynamics and time-resolved fluorescence of azobenzene in solution: a mixed quantum-classical simulation. *J. Am. Chem. Soc.*, 133:5109–5123, 2011.

[26] O. Weingart, Z.G. Lan, A. Koslowski, and W. Thiel. Chiral pathways and periodic decay in cis-azobenzene photodynamics. *J. Phys. Chem. Lett.*, 2:1506–1509, 2011.

[27] J.A. Gámez, O. Weingart, A. Koslowski, and W. Thiel. Cooperating dinitrogen and phenyl rotations in trans-azobenzene photoisomerization. *J. Chem. Theory Comput.*, 8:2352–2358, 2012.

[28] M. Böckmann, S. Braun, N.L. Doltsinis, and D. Marx. Mimicking photoisomerisation of azo-materials by a force field switch derived from nonadiabatic ab initio simulations: Application to photoswitchable helical foldamers in solution. *J. Chem. Phys.*, 139:084108, 2013.

[29] L. Verlet. Computer" experiments" on classical fluids. I. Thermodynamical properties of Lennard-Jones molecules. *Phys. Rev.*, 159:98, 1967.

[30] B. Hess, H. Bekker, H.J.C. Berendsen, and J.G.E.M. Fraaije. LINCS: a linear constraint solver for molecular simulations. *J. Comput. Chem.*, 18:1463–1472, 1997.

[31] M. Böckmann, C. Peter, L.D. Site, N.L. Doltsinis, K. Kremer, and D. Marx. Atomistic force field for azobenzene compounds adapted for QM/MM simulations with applications to liquids and liquid crystals. *J. Chem. Theory Comput.*, 3:1789–1802, 2007.

[32] H.J.C. Berendsen, J.P.M. Postma, W.F. van Gunsteren, A.R.H.J. DiNola, and J.R. Haak. Molecular dynamics with coupling to an external bath. *J. Chem. Phys.*, 81(8):3684–3690, 1984.

[33] T. Pancur, F. Renth, F. Temps, B. Harbaum, A. Krüger, R. Herges, and C. Näther. Femtosecond fluorescence up-conversion spectroscopy of a rotation-restricted azobenzene after excitation to the S_1 state. *Phys. Chem. Chem. Phys.*, 7:1985–1989, 2005.

[34] M. Böckmann, N.L. Doltsinis, and D. Marx. Nonadiabatic hybrid quantum and molecular mechanic simulations of azobenzene photoswitching in bulk liquid environment. *J. Phys. Chem. A*, 114:745–754, 2009.